

Structure-Based Design of Novel Chk1 Inhibitors: Insights into Hydrogen Bonding and Protein–Ligand Affinity

Nicolas Foloppe,* Lisa M. Fisher, Rob Howes, Peter Kierstan, Andrew Potter, Alan G. S. Robertson, and Allan E. Surgenor

Vernalis (R&D) Limited, Granta Park, Abingdon, Cambridge CB1 6GB, U.K.

Received December 1, 2004

We report the discovery, synthesis, and crystallographic binding mode of novel furanopyrimidine and pyrrolopyrimidine inhibitors of the Chk1 kinase, an oncology target. These inhibitors are synthetically tractable and inhibit Chk1 by competing for its ATP site. A chronological account allows an objective comparison of modeled compound docking modes to the subsequently obtained crystal structures. The comparison provides insights regarding the interpretation of modeling results, in relationship to the multiple reasonable docking modes which may be obtained in a kinase-ATP site. The crystal structures were used to guide medicinal chemistry efforts. This led to a thorough characterization of a pair of ligand–protein complexes which differ by a single hydrogen bond. An analysis indicates that this hydrogen bond is expected to contribute a fraction of the 10-fold change in binding affinity, adding a valuable observation to the debate about the energetic role of hydrogen bonding in molecular recognition.

Introduction

Control of the cell cycle provides potential targets for the development of therapeutics against cancer.¹ A key point in the cell cycle is the checkpoint between the G2 and the M phases (G2/M).² This checkpoint is a pathway controlling the ability of eukaryotic cells to arrest the cell cycle in G2 in response to DNA damage, to allow time for DNA repair.^{3,4} DNA damage may be due to radiation or chemical agents, which are still a major component of cancer therapy. Key to the relevance of the G2/M checkpoint for cancer treatment is that, in normal cells, DNA damage also triggers cell cycle arrest in the G1 phase, via the tumor suppressor protein p53.^{5,6} This G1/S checkpoint is impaired in many tumor cells, because of mutations in p53,^{5,7} and these tumor cells can only rely on the G2/M checkpoint to repair their DNA in response to DNA damaging agents. Therefore, abrogation of the G2/M checkpoint in these tumor cells would allow premature mitotic entry in the presence of DNA damage, leading ultimately to cell death. In contrast, normal cells would arrest in G1 and would be minimally affected by abrogation of the G2/M checkpoint. Therefore, inhibition of the G2/M checkpoint should lead to an increased and selective sensitivity of cancer cells to DNA damaging agents,^{8,9} suggesting that small molecule inhibitors of this checkpoint may prove useful in cancer therapy as sensitizing agents.^{6,10,11}

Arrest in G2 is mainly regulated by the maintenance of inhibitory phosphorylation on cyclin-dependent kinase 1 (CDK1) (also called Cdc2), which prevents activation of this mitosis promoting CDK.^{12–14} Dephosphorylation, and thereby activation, of CDK1 is carried out in human cells by the dual specificity phosphatase Cdc25C.^{15,16} Cdc25C can be phosphorylated on Ser216

by the human nuclear serine/threonine kinase Chk1.¹⁷ This phosphorylation is necessary for arrest in G2 in response to DNA damage in human cells¹⁸ and promotes binding of the 14-3-3 protein to Cdc25C, which in turn prevents Cdc25C from interacting functionally with CDK1.¹⁸ These biochemical results are consistent with genetic studies.^{19–22} Chk1 is activated in response to DNA damage via the ATM/ATR pathway^{23–26} and is required for checkpoint arrest.²⁷ Inhibition of Chk1 may also induce apoptosis.²⁰ In sum, there is ample biological evidence that Chk1 plays an essential role in the regulation of the G2/M checkpoint,^{4,23,28–30} suggesting that the inhibition of Chk1 should abrogate this checkpoint in a manner relevant to the treatment of cancer.⁶ Selective Chk1 inhibitors should also prove useful to study the regulation of the G2/M checkpoint.

Several Chk1 inhibitors are already known, including natural products such as staurosporine (and its derivatives: 7-hydroxystaurosporine (UCN-01),^{31,32} indolocarbazole analogues,^{33,34} isogranulatimide,³⁵ and Gö6976³⁶) and debromohymenialdisine.³⁷ This is consistent with some of these compounds being potent abrogators of the G2/M checkpoint in cells,^{8,33,37} adding to the relevance of Chk1 as an oncology target. UCN-01 is indeed undergoing clinical trials as an anticancer agent.^{38,39} A limited number of additional Chk1 inhibitors have been reported;^{6,40,41} however, there is clearly a need to identify more druglike Chk1 inhibitors, given the typical attrition rate in drug discovery. This should be facilitated by the structural information available for the Chk1 kinase domain.

Chk1 is a 54 kDa protein of 476 amino acids¹⁷ comprised of a highly conserved N-terminal kinase domain (residues 1–265) followed by a linker and a less conserved C-terminal region that decreases Chk1 kinase activity.⁴² The crystal structure of the kinase domain of human Chk1 and its complex with the ATP analogue AMP-PNP have been solved at 1.7 Å resolution.⁴²

* To whom correspondence should be addressed: N. Foloppe, Vernalis (R&D) Ltd., Granta Park, Abingdon, Cambridgeshire CB1 6GB, U.K.; phone (direct): + (44) (0) 1223 895 338; fax: + (44) (0) 1223 895 556; email: n.foloppe@vernalis.com.

Crystal structures of Chk1 complexed with ATP-competitive inhibitors staurosporine, 7-hydroxystaurosporine (UCN-01), and SB-218078 have also been presented.⁴³ This puts structure-based inhibitor design strategies against human Chk1 kinase on firm footing.

This work presents the discovery and elaboration of a new type of druglike ATP-competitive Chk1 inhibitor, in the context of the crystal structures of these molecules bound to the ATP site. These structures allowed to rationalize the structure–activity relationship (SAR) around the initial chemotype and to improve its affinity by modification of their scaffold. This work also drew on the iterative nature of molecular modeling as part of structure-based drug design against a kinase, which is frequently referred to but rarely illustrated. Finally, these results enabled us to specifically probe the strength of a hydrogen bond between compounds and the highly conserved kinase motif with which most ATP-competitive ligands interact. This interaction is found to be moderately favorable, and this should contribute to a better characterization of the much debated role of the energetics of hydrogen bonding for the binding affinity of ligands to proteins.

Results and Discussion

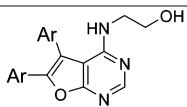
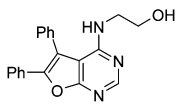
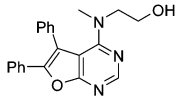
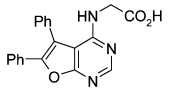
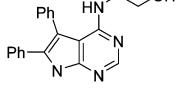
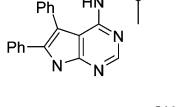
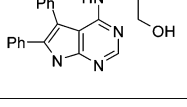
This report lends itself to a chronological presentation, which puts into perspective the influence of the structural information on the medicinal chemistry strategy.

Identification of a Novel Chk1 Inhibitor. Compound **1** (Table 1) was identified as an inhibitor of human Chk1 during a medium throughput screen of a commercial library of compounds provided by Chemical Diversity (ChemDiv).⁴⁴ In that screen, compound **1** inhibited Chk1 with an IC_{50} of 15.4 μ M. It was further shown that compound **1** inhibits Chk1 in an ATP-competitive manner by standard kinetic methods, with a K_i of 7.2 μ M.

A search of the Vernalis electronic catalog of commercially available compounds⁴⁵ identified four analogues (**8–11**, Table 2) of compound **1** which were obtained and assayed. This search aimed to identify compounds containing the same chemical core (5,6-diphenyl-furo[2,3]pyrimidin-4-ylamine, represented by compound **8**) as compound **1**, using the substructure search algorithm implemented in the MDL ISIS/Base software.⁴⁶ The other analogues (**12–15**) of compound **1** shown in Table 2 were synthesized in-house following published procedures⁴⁷ (Scheme 1). Thus, condensation of the commercially available aminofuran (**16**), with in situ generated acetic formic anhydride gave the N-formyl derivative (**17**). This was cyclized under thermal conditions giving the oxo-compound (**18**) in good yield. Chlorination was easily effected using phosphorus oxychloride producing derivative **19** in 75% yield. Displacement of the chlorine was achieved in refluxing ethanol with 2 equiv of the corresponding amine, leading to the furanopyrimidine product (**20**) in 70–80% yield.

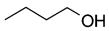
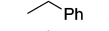
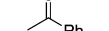
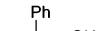

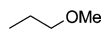

The analogues in Table 2 differ from compound **1** by the lack of methoxy substituents and the alteration of the hydroxy-ethyl side chain, which led to a systematic loss of affinity. A structure-based strategy was then pursued to explain this initial SAR and suggest more successful ways to elaborate compound **1**.

Table 1. Structure and Binding Affinities of Chk1 Inhibitors

Compound	Structure	IC_{50} (μ M) ^a			K_i (μ M)
		Chk1	PKA	CDK1	Chk1
1 ^b		15.4	>200	29.4	7.2
2		20.9	>200	>200	13.7 ^c
3		6.1	>200	111.4	-
4		22.9	>200	>200	-
5		2.3	>200	5.0	1.3 ^c
6		5.5	>200	3.7	-
7		1.4	>200	1.5	-

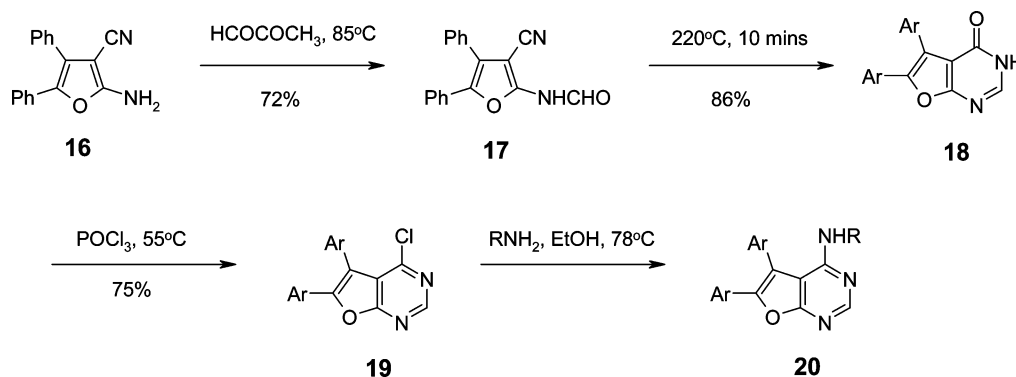
^a Measured for human PKA and CDK1, in addition to Chk1 kinase, to explore binding selectivity. ^b Ar is *p*-OMe phenyl. ^c Each of these K_i was derived from three independent sets of measurements; the associated standard deviations were 4.5 and 1.3 μ M for compounds **2** and **5**, respectively.

Table 2. Inactive^a Analogues of Compound **1**

Compound	R
8	H
9	
10	
11	
12	
13	
14	
15	

^a Defined as having an IC_{50} > 100 μ M for Chk1. These analogues differed by the nature of the listed R groups, as part of the chemical structure shown.

Initial Structural Model. Given that in-house Chk1 X-ray crystallography was not yet available at the outset of the project, compound **1** was docked to a publicly

Scheme 1. Synthesis of Furanopyrimidine Derivatives

available X-ray structure⁴² using molecular modeling techniques. This yielded two interesting putative binding modes (Figure 1) where compound **1** was well buried in the ATP-binding site, while forming hydrogen bonds

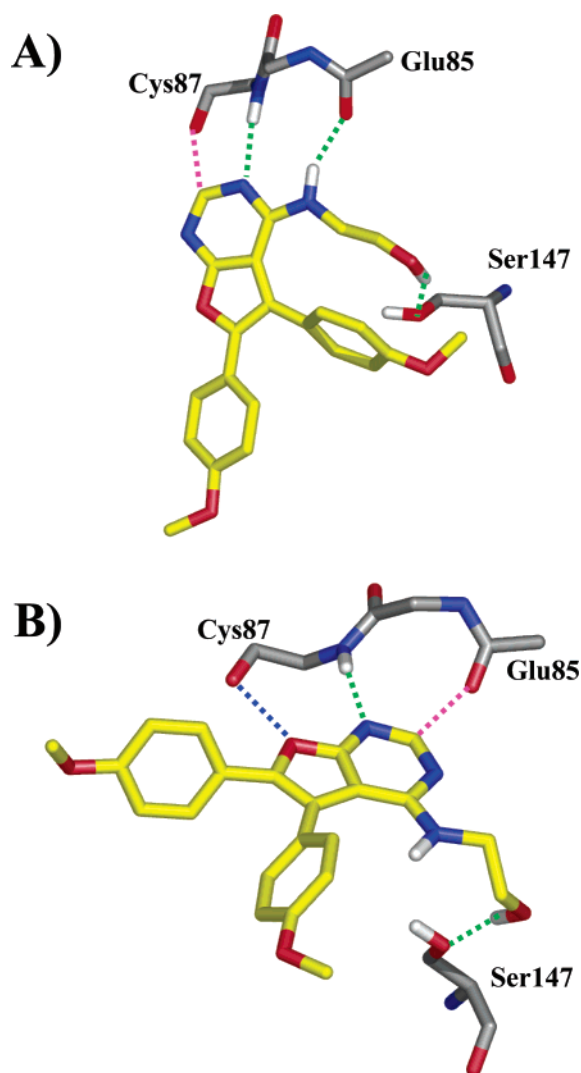


Figure 1. The two initial docking modes selected for compound **1**. The best scoring docking mode is shown in panel **A**. For both docking modes, the kinase hinge backbone (Glu85 and Cys87) is shown. Ser147 is also shown because it is hydrogen bonded by the hydroxy-ethyl side chain. Other residues and most hydrogens were omitted for clarity. Classical hydrogen bonds are depicted with green dotted lines, while C—H...O hydrogen bonds are traced in magenta. In docking mode **B**, the contact between the furan oxygen and the carbonyl oxygen of Cys87 is shown with a blue dotted line.

with the highly conserved backbone kinase motif at the hinge between the two lobes of the kinase domain. These hydrogen bonds are observed with almost all other kinase inhibitors.^{48–50} The methoxy groups pointed away from the active site and toward the solvent, suggesting that it was not the lack of these groups which imparted a loss of activity in the compounds shown in Table 2. On the other hand, in both docking modes the hydroxy-ethyl side chain had the correct length to hydrogen bond to the hydroxyl oxygen of Ser147. This was encouraging because it could possibly explain why extending this side chain by one methylene group abolished binding to Chk1. In particular, systematic attempts to accommodate a hydroxy-propyl side chain instead of its hydroxy-ethyl analogue, while keeping docking mode **A**, resulted in severe steric clashes between the side chain and the protein. Also, three hydrogen bonds with the kinase hinge backbone were formed in docking mode **A**, although only two were formed in mode **B**. Some of these hydrogen bonds were C—H...O hydrogen bonds involving a polarized C—H bond of the pyrimidine moiety (Figure 1), the existence of which is well documented.^{51–53} Another feature in favor of docking mode **A** was the presumably unfavorable interaction between the furan oxygen and the carbonyl oxygen of Cys87 in docking mode **B**. Also, there was skepticism about the orientation of the amino N—H bond in mode **B**, where it points toward a phenyl ring of the same compound. Although such favorable polar interactions involving the π electrons of aromatic moieties are known to exist,^{54–56} it was initially deemed unlikely in the present context, assuming that a stronger hydrogen bond could be formed with a carbonyl backbone in mode **A**. In addition, the methoxy group closest to Ser147 accepted a hydrogen bond from Lys38 in docking mode **A** (not shown), with no counterpart for this interaction in mode **B**. Given that the two docking modes buried approximately the same amount of apolar surface area, mode **A** scored more favorably than mode **B**, because of its apparently more favorable polar interactions. Finally, there was no room for substituents around the hydroxy-ethyl side chain in mode **A**, which was consistent with the available SAR (Table 2); that is, all of the substituted analogues of this side chain had lost binding to Chk1. Docking mode **A** was therefore adopted as a convincing initial structural working hypothesis for medicinal chemistry efforts.

Test and Revision of the Initial Structural Model. In both docking modes **A** and **B**, the methoxy groups are at the periphery of the binding site, pointing toward

Table 3. Crystallographic Data Collection and Refinement Statistics for Chk1 in Complex with Compounds 1–7

structure	Chk1 + compound						
	1	2	3	4	5	6	7
Data Collection Statistics							
resolution (Å)	2.00	2.10	2.10	2.10	2.12	2.80	2.20
measured reflections	54186	144361	49021	51083	50424	196243	48914
unique reflections	21797	20050	18386	19953	17903	7714	16331
completeness: overall/in hrb ^c (%)	95.1/95.1	96.6/83.2	99.1/99.0	96.7/90.1	96.1/89.7	97.9/98.9	96.3/89.4
average multiplicity/in hrb	2/1	4/2	3.2/1.0	4.1/3.6	5.1/4.5	3.2/3.2	4.3/1.3
mean I/σ: overall/in hrb	14.5/3.6	13.0/2.7	6.7/1.0	13.6/3.5	10.2/3.4	9.1/1.0	7.6/2.7
R _{merge} : overall/in hrb (%)	4.4/22.9	8.4/43.8	9.1/42.7	6.3/31.3	5.0/30.6	12.9/50.9	7.7/39.1
Refinement Statistics							
R _{free} ^a (%)	22.6	24.5	29.4	25.7	28.1	28.5	27.9
R _{cryst} (%)	16.3	18.3	20.7	17.6	22.6	20.3	19.8
rms deviations: ^b	0.016	0.017	0.027	0.023	0.021	0.024	0.015
bonds (Å)	1.6	1.6	2.4	2.1	2.5	2.4	1.6
angles (deg)	2.3	2.8	2.3	2.6	2.8	3.1	2.3
B factor (Å ²)							
PDB code	2BR1	2BRB	2BRG	2BRH	2BRM	2BRN	2BRO

^a R_{free} is the R factor calculated using 5% of the reflection data chosen randomly and omitted from the refinement process, whereas R_{cryst} is calculated with the remaining data used in the refinement. ^b The rms bond lengths and angles are the deviations from ideal values; the rms deviation in B factors is calculated between covalently bonded atoms. ^c Highest resolution bin.

the solvent. Although one of these methoxy groups was hydrogen bonded to Lys38 in mode **A**, this interaction was not expected to contribute significantly to the affinity of the compound for the site, given the intrinsic flexibility of the lysine side chains and the competition by water for this solvent-exposed site. It was therefore predicted that if either mode **A** or **B** were correct, an analogue (compound **2**, Table 1) lacking the methoxy groups (while keeping the original hydroxy-ethyl side chain) would have an affinity similar to that of compound **1**. A more stringent test of docking mode **A**, however, was to methylate the amino nitrogen (compound **3**) presumed to hydrogen bond the carbonyl oxygen of Glu85.

Compounds **2** and **3** were synthesized with high priority, as described above and in Scheme 1. As predicted, compound **2** was virtually as active as compound **1** with respect to Chk1 (Table 1). Compound **3**, however, was slightly more active than compounds **1** and **2**. This implied that docking mode **A** was not correct, but uncertainty remained about mode **B**, given some of its peculiarities. In-house X-ray crystallography, however, confirmed the overall relevance of this binding mode.

Experimental Binding Mode. The crystal structures of compounds **1**, **2**, and **3** bound to Chk1 were solved, with resolutions and refinement statistics given in Table 3. These compounds were found to bind in the ATP-binding site, consistent with the observation that they are competitive inhibitors. These structures revealed the same overall binding mode (Figure 2) for compounds **1**, **2**, and **3**. In view of this experimental binding mode, docking mode **B** correctly predicted the main contacts between the compound and the kinase backbone and the intramolecular orientation of the amino N–H bond toward the phenyl ring. The distance (3.7 Å) between this amino nitrogen and the centroid of the phenyl ring and the N–H⋯centroid angle (149.0°) are compatible with an interaction with some hydrogen bond character where the phenyl ring acts as an acceptor.^{54–56} Another likely acceptor is the water molecule positioned 3.1 Å from the amino nitrogen (N–H⋯O angle of 126.8°). Polar interactions involving phenyl rings as acceptors are typically not represented

in current docking scoring functions,⁵⁷ and yet the present results indicate that they are relevant to drug design. It is interesting to note that the polar character of this interaction can be changed to a completely apolar interaction with only minor structural adjustments, as seen in the structure of compound **3**, where the methyl group branching off the amino nitrogen packs against the face of the phenyl (not shown). The possibility for such dual character may help interpret apparently surprising SAR data in other contexts. Other interesting interactions present in the X-ray binding mode include the contacts between the two phenyl carbon atoms and the carbonyl oxygen of Cys87 (Figure 2). The orientation of these phenyl C–H bonds toward the carbonyl oxygen suggests that they are favorable interactions.^{52,53,58} This is supported by the observation of similar interactions involving Phe237 and the carbonyl oxygen of Val123 in protein kinase A (PKA) (Figure 5).

The main difference between docking mode **B** and its experimental counterpart is in the positioning of the compound hydroxy-ethyl side chain. In the crystal structures, the distance between the hydroxyl oxygen of the compound and Ser147 is ~4.2 Å, indicating that there is no hydrogen bond between these groups, in contrast to model **B**. Instead, the compound hydroxyl forms an intramolecular hydrogen bond with one of the pyrimidine nitrogens (Figure 2) with an oxygen to nitrogen distance of 3.0 Å. The compound side chain adopts a more staggered conformation in the crystal structure than in docking mode **B**, which contributes to explain why the intramolecular hydrogen bond is preferred.

The crystallographic conformation of the hydroxy-ethyl side chain explains, by and large, the lack of binding of the compounds listed in Table 2. Clearly, the modifications to the hydroxy-ethyl side chain in compounds **9**, **10**, **11**, and **14** would disrupt the associated intramolecular hydrogen bond, with no alternative favorable interactions between the side chain and the protein. The lack of binding of compounds **12** and **15** can be explained by steric clashes between the added methyl (**15**) or phenyl (**12**) groups with the side chains of Val23 or Leu84. The side chain of compound **14** would also be poorly accommodated in the binding site.

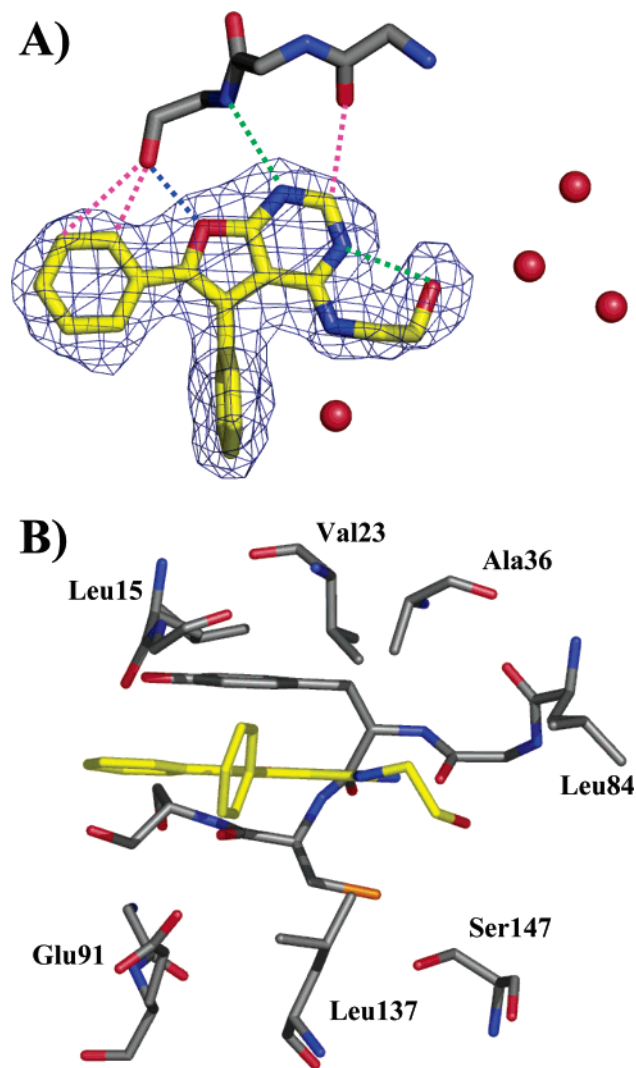


Figure 2. Crystallographic binding mode of compound **2** in the ATP-binding site of Chk1. Panel A shows the compound $2F_o - F_c$ electron density contoured at 2.0σ (calculated for the final refined structure) and the interactions between the compound and the kinase hinge backbone. Classical hydrogen bonds are depicted with green dotted lines, while C–H...O hydrogen bonds are traced in magenta. The contact between the furan oxygen and the carbonyl oxygen of Cys87 is shown with a blue dotted line. Water molecules are shown as red spheres, including the water located 3.1 \AA from the amino nitrogen and the three waters in the targeted pocket (see main text). Panel B shows the same binding mode viewed in the plane of the compound aromatic scaffold with selected residues labeled.

A more general lesson from this binding mode is that suboptimal protein–ligand interactions ought to be tolerated to some degree in virtual screening scoring functions used at the hit discovery stage, which is typically concerned with the discovery of ligands with initial affinities in the micromolar range. This is illustrated by the contact between the furan oxygen of compounds **1–3** and the carbonyl oxygen of Cys87, which are about 3.2 \AA apart in the crystal structures. The targeted manipulation of this interaction led to improvement of the binding affinity of the series for Chk1.

Alternate Binding Modes as a Test for More Sophisticated Calculations. The initial docking mode **A** of compound **1** (Figure 1) was obtained with a docking empirical scoring function. Such functions are typically

optimized toward computational speed, to allow the virtual screening of large collections of compounds, and are also commonly used to propose structural hypotheses for ligand design. Because of speed requirements, these scoring functions involve a number of well-known approximations⁵⁷ in their treatment of molecular recognition, in particular with respect to electrostatics. A more physically sound (but more computationally demanding) approach termed MM/PBSA (molecular mechanics/Poisson–Boltzmann surface area) has recently emerged as a promising technique for improved predictions of protein–ligand interactions.^{59–61} A rigorous treatment of electrostatics, which accounts for desolvation upon complex formation, is a key feature of MM/PBSA calculations.

It is important to test if these calculations can help discriminate between different docking modes of the same ligand, but only limited work has been presented in that direction.⁶¹ It is therefore interesting to investigate whether an MM/PBSA protocol could rank the X-ray binding mode and docking mode **B** more favorably than docking mode **A**, especially because mode **A** was initially preferred to mode **B** on the basis of a count of polar (electrostatic) interactions. The calculations were performed with both compounds **1** and **2**, to assess the robustness of the results. Indeed, in docking mode **A**, a methoxy group of compound **1** is hydrogen bonded to the amino group of Lys38, but this interaction is not present with compound **2**. In the MM/PBSA framework, the total free energy of binding $\Delta G_{\text{binding}}$ can be decomposed into electrostatic (ΔG_{elec}), van der Waals (ΔG_{vdw}), and nonpolar (ΔG_{np}) components. The electrostatic part includes both ligand–protein interactions and solvation effects, while the nonpolar contribution is usually interpreted as representing the hydrophobic effect.^{59–61} Because we aimed to compare different binding modes, we needed to take into account the internal conformational energy of the ligand ($\Delta G_{\text{internal_rel}}$). Only relative values of $\Delta G_{\text{binding}}$ are required, and it is therefore reasonable to neglect the entropic contributions (see Methods Section). It follows that

$$\Delta G_{\text{binding}} = \Delta G_{\text{elec}} + \Delta G_{\text{vdw}} + \Delta G_{\text{np}} + \Delta G_{\text{internal_rel}} \quad (\text{a})$$

The various components to $\Delta G_{\text{binding}}$ for compounds **1** and **2** in their X-ray binding mode and docking modes **A** and **B** are given in Table 4. It should be noted that $\Delta G_{\text{binding}}$ is not appropriate to compare binding affinities of compounds **1** and **2** because the internal energetics of the ligands would cancel out in such a comparison. The contribution of ΔG_{elec} was calculated for two values of the solute dielectric constant ϵ , to test the effect of this parameter on the results. The choice of ϵ affects the absolute values of ΔG_{elec} , but has much less impact on the corresponding differences between binding modes, and does not alter the relevant rankings. In all cases, ΔG_{elec} acts against binding, reflecting the importance of desolvation. It is interesting to note that for compound **2** ΔG_{elec} favors the X-ray binding mode over docking mode **A**, despite a presumed electrostatic clash between the furan and the carbonyl oxygens in the X-ray structure. ΔG_{np} also favors the X-ray binding mode over docking mode **A**, although by a small margin. The largest contribution opposing docking mode **A** is from $\Delta G_{\text{internal_rel}}$. This is consistent with the presence of an

Table 4. Relative MM/PBSA Energetics^a of Compounds **1** and **2** in the X-ray Binding Mode^b and in Docking Modes **A** and **B**

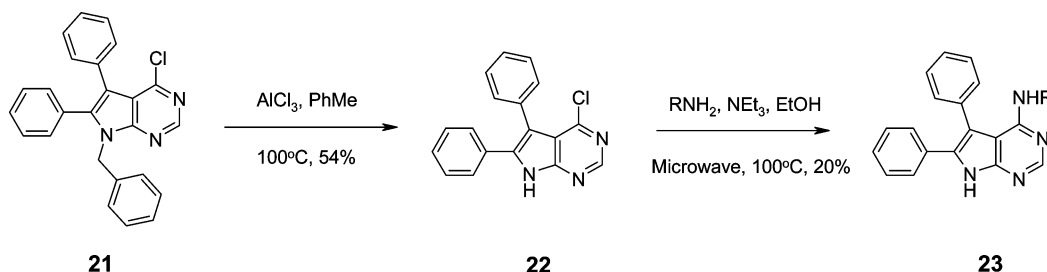
	ΔG_{elec}	ΔG_{vdw}	ΔG_{np}	$\Delta G_{\text{internal_rel}}$	$\Delta G_{\text{binding}}$	$\Delta\Delta G_{\text{binding}}$
compound 1						
X-ray ^b	11.7 ($\epsilon = 2$)	-39.7	-22.4	0.0 ^c	-50.4 ($\epsilon = 2$)	
	6.0 ($\epsilon = 4$)				-56.1 ($\epsilon = 4$)	
docking mode A	7.8 ($\epsilon = 2$)	-40.3	-21.5	14.3	-39.7 ($\epsilon = 2$)	10.7 ($\epsilon = 2$)
	3.5 ($\epsilon = 4$)				-44.0 ($\epsilon = 4$)	12.1 ($\epsilon = 4$)
docking mode B	9.2 ($\epsilon = 2$)	-37.5	-22.7	2.0	-49.0 ($\epsilon = 2$)	1.4 ($\epsilon = 2$)
	4.6 ($\epsilon = 4$)				-53.6 ($\epsilon = 4$)	2.5 ($\epsilon = 4$)
compound 2						
X-ray ^b	7.2 ($\epsilon = 2$)	-36.2	-20.2	0.0 ^c	-49.2 ($\epsilon = 2$)	
	3.5 ($\epsilon = 4$)				-52.9 ($\epsilon = 4$)	
docking mode A	8.1 ($\epsilon = 2$)	-38.6	-19.6	21.3	-28.8 ($\epsilon = 2$)	20.4 ($\epsilon = 2$)
	4.3 ($\epsilon = 4$)				-32.6 ($\epsilon = 4$)	20.3 ($\epsilon = 4$)
docking mode B	8.4 ($\epsilon = 2$)	-38.7	-19.7	3.7	-46.3 ($\epsilon = 2$)	2.9 ($\epsilon = 2$)
	3.8 ($\epsilon = 4$)				-50.9 ($\epsilon = 4$)	2.0 ($\epsilon = 4$)

^a All energies are in kcal/mol. ΔG_{elec} is reported for a solute dielectric constant ϵ of 2 or 4. $\Delta\Delta G_{\text{binding}} = \Delta G_{\text{binding}}(\text{X-ray}) - \Delta G_{\text{binding}}(\text{docking mode})$. ^b Refers to the X-ray conformation of the ligand, not the X-ray coordinates of the protein–ligand complex. Calculations reported in this table were obtained with the protein X-ray structure 1IA8 from the PDB, used to generate docking modes **A** and **B**. ^c Internal energies are differences relative to the most stable internal energy, set to 0.0.

Table 5. Binding Free Energies^a of Compounds **2** and **5** Calculated with MM/PBSA

	protein structure ^b	ΔG_{elec}	ΔG_{vdw}	ΔG_{np}	$\Delta G_{\text{binding}}$
compound 2	protein X-ray structure solved with cpd 2	4.4 ($\epsilon = 2$)	-37.3	-19.2	-52.1 ($\epsilon = 2$)
	“native X-ray structure”	2.4 ($\epsilon = 4$)			-54.1 ($\epsilon = 4$)
	protein X-ray structure solved with cpd 5	5.5 ($\epsilon = 2$)	-37.9	-19.8	-52.2 ($\epsilon = 2$)
	“exchanged X-ray structure”	2.3 ($\epsilon = 4$)			-55.4 ($\epsilon = 4$)
compound 5	protein X-ray structure solved with cpd 5	4.1 ($\epsilon = 2$)	-38.0	-19.4	-53.3 ($\epsilon = 2$)
	“native X-ray structure”	2.2 ($\epsilon = 4$)			-55.2 ($\epsilon = 4$)
	protein X-ray structure solved with cpd 2	4.2 ($\epsilon = 2$)	-36.7	-9.1	-51.6 ($\epsilon = 2$)
	“exchanged X-ray structure”	1.6 ($\epsilon = 4$)			-54.2 ($\epsilon = 4$)

^a All energies are in kcal/mol. ΔG_{elec} is reported for a solute dielectric constant ϵ of 2 or 4. ^b Protein X-ray structure used in the calculations.

Scheme 2. Synthesis of Pyrrolopyrimidine Derivatives

intramolecular hydrogen bond in the experimental binding mode, without a counterpart in docking mode **A**. This, however, is not enough to explain differences of > 10.0 kcal/mol in $\Delta G_{\text{internal_rel}}$ between docking mode **A** and the other two modes. Additional analysis revealed that these large differences also reflect unfavorable van der Waals contacts between the hydroxy-ethyl side chain and the adjacent phenyl ring in docking mode **A** (Figure 1). Recalculation of the $\Delta G_{\text{internal_rel}}$ contributions with the Merck molecular force field⁶² confirmed the trends in $\Delta G_{\text{internal_rel}}$ obtained with the CHARMM force-field between binding mode **A** and the other modes (not shown). One, however, could not rule out docking mode **A** solely on the basis of its high internal strain energy.⁶³ The net result is values of $\Delta G_{\text{binding}}$ which clearly favor the X-ray binding mode over docking mode **A**, by a difference of $\Delta\Delta G_{\text{binding}}$ which is > 10.0 kcal/mol (Table 4). These calculations also clearly discriminate between docking modes **A** and **B**, in favor of the latter. $\Delta G_{\text{binding}}$ also favors slightly the X-ray binding mode over docking mode **B** but by differences which may be of the same order as the error margin of the calculations. Overall, these results stress the importance of a detailed treatment of the intramolecular energetics in scoring func-

tions and confirm that the MM/PBSA strategy holds promise to discern between multiple docking modes of a same compound.

Structure-Based Design. To improve the affinity of the furanopyrimidine series (compounds **1–4**) for Chk1, the first suggestion was to replace the furan by a pyrrole in its scaffold. Indeed, simple visualization of the crystal structures suggested that replacing the furan oxygen by a pyrrole N–H would create an additional hydrogen bond between the ligand scaffold and the protein. This led us to synthesize compound **5**, with a pyrrolopyrimidine scaffold (Table 1).

The pyrrolopyrimidines were prepared from the commercially available analogue **21** (Scheme 2). This was debenzylated with aluminum chloride in refluxing toluene to give the derivative **22** in 54% yield, based on the recovered starting material. The anilino derivatives were prepared by microwave irradiation of precursor **22** with 6 equiv of the corresponding amine in ethanol at 100 °C. Purification of the crude material using column chromatography gave the pure pyrrolopyrimidines in 10–20% yield.

Compound **5** led to a 10-fold increase in binding affinity to Chk1 over compound **2** (Table 1). The crystal

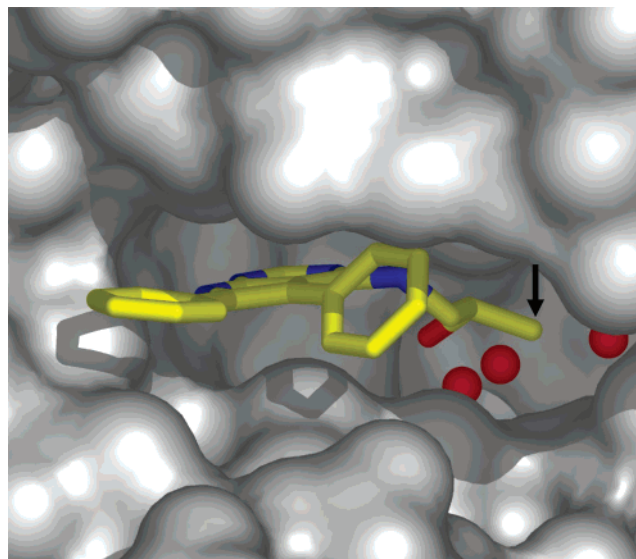


Figure 3. Crystal structure of compound **6** bound to Chk1. The protein is represented as a gray molecular surface. The black arrow points to the methyl group added to the hydroxyethyl side chain. This methyl group projects toward a buried pocket which contains three water molecules (red spheres).

structure of compound **5** bound to Chk1 confirmed that the pyrrole N–H hydrogen bonds to the backbone carbonyl of Cys87, with standard geometries (N \cdots O distance = 3.1 Å, N \cdots O–C angle = 126.8°). The implications of this result for the contribution of hydrogen bonds to the association free energy of ligand–protein complexes are discussed further below. Another strategy to improve the affinity of the compounds to Chk1 would be to target a pocket located in the vicinity of the ligand hydroxyethyl side chain (Figures 2 and 3). This pocket is lined by Asn59, Leu84, and Phe149, and the electron density defining the crystal structure shows that three water molecules occupy the pocket in the present ligand–Chk1 complexes. This region is a potentially attractive target for gaining potency against Chk1 because this pocket is well buried at the bottom of the ATP-binding site (Figure 3) and should allow the formation of additional tight interactions between ligand and protein. It might also be entropically favorable to displace the water molecules present in the pocket into the bulk solvent.⁶⁴

To reach into this pocket of interest, simple proximity considerations dictate that derivatization of the compound's hydroxyethyl side chain is the only option available (Figures 2 and 3). In this side chain, the C–H vectors emanating from the carbon bound to the amino group do not point in directions which could be used to reach the pocket. One of the C–H vectors from the other side chain carbon, however, is projected in a direction which could be amenable to derivatization toward the pocket. The second C–H vector from the same carbon could allow targeting of Leu137 and Ser147, which would provide another region of interest to make additional interactions with the protein. Given the strict geometric constraints imposed by the protein environment, it was decided to adopt a stepwise approach, whereby the hydroxyethyl side chain would be derivatized incrementally rather than add complex substituents from the start. This should allow us to obtain useful

intermediary compounds, the crystal structures of which would act as a guide to reach the next stage.

Addition of a methyl group to compound **5** gave compound **6** and led to an apparent slight decrease in affinity when tested as a racemate (Table 1). Given the introduction of a chiral center in compound **6**, and that only one of these stereoisomers may bind to Chk1, the actual affinity of the active stereoisomer may be the same as that of compound **5**. Importantly, however, the crystal structure of compound **6** bound to Chk1 confirmed that the methyl group was added toward the targeted pocket (Figure 3). The associated crystallographic electron density could be interpreted such that only the *R* stereoisomer was bound to Chk1. Compound **7** was made by building on compound **6**, with the intention that the added hydroxyl group may hydrogen bond to Ser147. This was, however, not observed in the crystal structure of compound **7**, where the added hydroxyl group points away from both Ser147 and from the nearby pocket. Therefore, additional efforts will be needed to test if this pocket can be filled, with a concomitant favorable impact on the binding affinities. It remains, however, that this work presents significant progress toward that goal.

Experimental Probing of the Strength of a Protein–Ligand Hydrogen Bond. Like in the field of protein folding and stability,^{65,66} the net energetic contribution of ligand–protein hydrogen bonds to the binding affinity of these complexes has raised immense interest^{67–73} and remains controversial.^{74–76} One aspect of the controversy is that the chemical functions which hydrogen bond in the complex are also expected to form hydrogen bonds with water when ligand and protein are dissociated. Therefore, it is sometimes argued that hydrogen bonds between solutes contribute very little, if at all, to their free energy of association in water.^{77,78} Experimental studies of these questions have been hampered by the difficulty of systematically adding or removing exactly one hydrogen bond in the complexes, and therefore report of such systems is of general interest. These questions are particularly intriguing with kinases because they have become widely targeted in a number of therapeutic areas and most of their ligands form several hydrogen bonds with their backbone in the hinge region.⁴⁹ The thoroughly measured binding affinities (Figure 4) combined with the virtually identical binding modes of compounds **2** and **5**, ascertained by crystallography, provide a rare opportunity to relate our results to these issues. The change from a furan in compound **2** to a pyrrole in compound **5** is arguably as minor as experimentally possible. Because this change does not add or remove any flexible torsion, no compound internal strain or conformational entropies are involved, not even an entropy loss associated with restraining a torsional motion of the hydrogen mediating the hydrogen bond.⁷⁹ Also, the protein is expected to undergo the same desolvation upon binding of each ligand. Changing the furan to a pyrrole adds a standard and buried hydrogen bond in the complex with compound **5**, while deleting an oxygen \cdots oxygen contact. In addition, a simple inventory of the hydrogen bonds present in the relevant equilibria⁶⁹ indicates that one hydrogen bond to the furan oxygen is lost when this oxygen is transferred from water to the protein binding

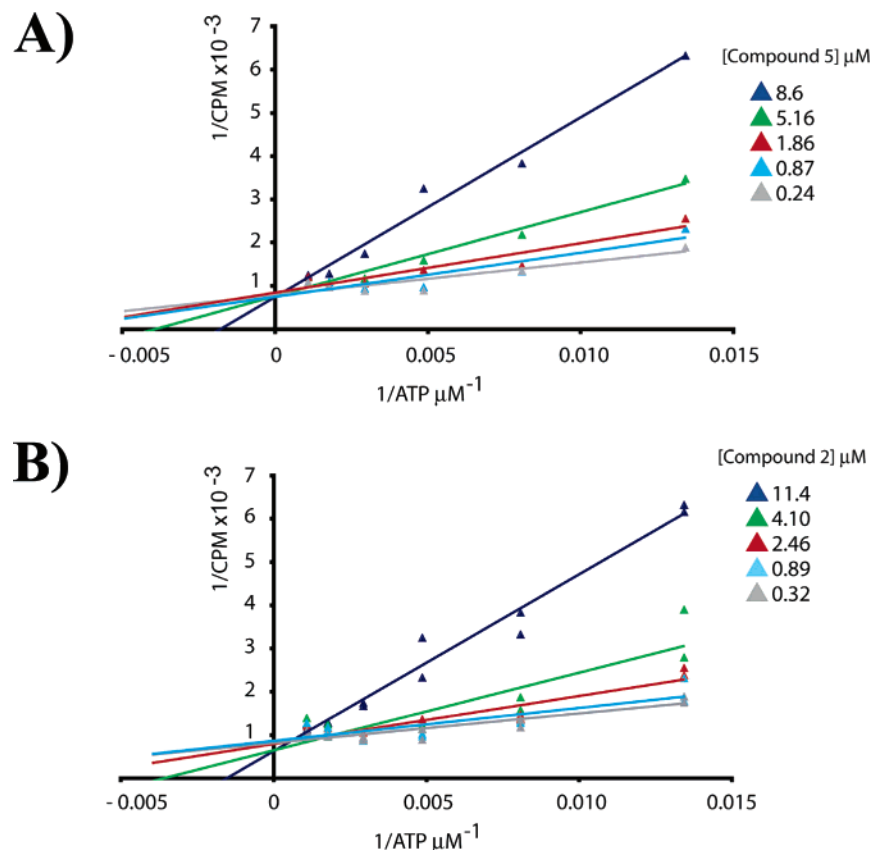


Figure 4. Double reciprocal (Lineweaver–Burke) plots using the Chk1 kinase assay, in the presence of compounds **5** (panel A) and **2** (panel B), showing the inverse of the reaction rate (1/CPM where CPM is the number of radioactive counts per minute) versus the inverse of the substrate concentration (1/[ATP]), with increasing inhibitor concentrations. The plots for each compound intersect on the 1/CPM axis, indicative of a simple competitive inhibitor. K_i values were determined by plotting the slopes of each plot against inhibitor concentration and the $-K_i$ value equaling the negative intercept on the y-axis (data not shown).

site, although there is no such loss with the pyrrole. Therefore, the higher affinity of compound **5** than that of compound **2** for the protein reflects the removal of unfavorable contributions to complex formation with compound **2**, as well as an additional hydrogen bond in the complex of compound **5**.

The difference in free energy of binding between these two complexes ($\Delta\Delta G$), derived from their K_i values with the law of mass action at the temperature of the experiments (303 K), yields $\Delta\Delta G = 1.4$ kcal/mol. A detailed physicochemical analysis of this result, including a dissection of enthalpic and entropic contributions, is beyond the scope of this work. Nevertheless, it is interesting to reflect on the practical implications of this result for ligand design. Given the above-mentioned differences regarding the relevant equilibria, it follows that the value of $\Delta\Delta G$ is an upper limit for the net contribution of the added hydrogen bond in the complex with compound **5**. This value is significantly less than the value of 4.0 kcal/mol reported in a similar comparison,^{67,68} possibly because the relatively weak hydrogen bond acceptor character of a furan oxygen⁸⁰ would facilitate its desolvation upon complex formation. Our observations are compatible with the 0.5–1.8 kcal/mol range derived for a neutral hydrogen bond for complex formation in an aqueous solvent.⁶⁹ They are also consistent with an analysis which concluded that the binding of balanol to PKA is mostly driven by the burial of nonpolar groups.⁶⁰ In sum, the present results add to the view that the net hydrogen-bonding energetics

favor the protein–ligand association only weakly. This is consistent with the components to the free energy of binding calculated for compounds **2** and **5**.

Computational Analysis of the Influence of the Added Hydrogen Bond on Binding. Hydrogen bonds are essentially electrostatic in nature. Therefore the MM/PBSA formalism, introduced above, should in principle allow us to dissect the atomistic contribution of a hydrogen bond to the free energy of association of a ligand and a protein. This may be approached by comparing the components to the free energy of binding for compounds **2** and **5** (Table 5). When the free energies of the binding of two distinct compounds are compared, the internal energy between bound and free ligand cancel out for each ligand, and $\Delta G_{\text{binding}}$ is reduced to

$$\Delta G_{\text{binding}} = \Delta G_{\text{elec}} + \Delta G_{\text{vdw}} + \Delta G_{\text{np}} \quad (\text{b})$$

Some authors^{60,81} have argued that the ΔG_{vdw} contribution is implicitly contained in ΔG_{np} , but this discussion has little bearing on the question at hand, because the influence of the hydrogen bond should be primarily reflected in ΔG_{elec} .

For both compounds **2** and **5**, $\Delta G_{\text{binding}}$ was calculated with the structure of the protein in which the compound was crystallized (“native X-ray structure”, Table 5), which yields slightly different components of $\Delta G_{\text{binding}}$ for compound **2** compared to those presented in Table 4. Values of $\Delta G_{\text{binding}}$ obtained with these native X-ray structures are more favorable for compound **5** than for

compound **2**, by about 1 kcal/mol, in agreement with the experimental results (see above). To isolate the contribution of the hydrogen bond of interest, however, it is desirable to compare compounds **2** and **5** with the same protein structure, which required additional calculations ("Exchanged X-ray structure", Table 5). Overall, the ΔG_{elec} contribution is only marginally more favorable with compound **5** than with compound **2**, which supports the view that the added hydrogen bond in the complex with compound **5** contributes only weakly to the free energy of association with the protein.

Although the protein structure is very similar whether crystallized with compound **2** or **5**, small structural differences are enough to impart variations to $\Delta G_{\text{binding}}$ of a given compound, which are on the same order as the differences in $\Delta G_{\text{binding}}$ between compounds. Because of these structure-dependent variations, it may be more accurate to extract the MM/PBSA energies from a thermally equilibrated ensemble of structures, such as those generated by molecular dynamics, but this is beyond the scope of this work. A detailed experimental characterization of the thermodynamics of binding of compounds **2** and **5** would also be highly valuable.

Selectivity. Different kinases are involved in a variety of cell signaling pathways,⁸² but X-ray structures combined with sequence alignments have shown that many features of the ATP-binding pocket tend to be conserved across kinases.^{48–50} Therefore selectivity of inhibition for a particular kinase is a well-known issue, and we initiated work to investigate this question for Chk1 and its inhibitors presented here (Table 1). Human PKA was used as a first test for selectivity because it is easily available and still closely related to Chk1 phylogenetically,⁸² with a 29% sequence identity between the two sequences (shortest sequence used for total length). The IC_{50} of Chk1 inhibitors **1–7** for PKA was > 200 mM, and this lack of inhibition for PKA can be understood in structural terms. An alignment of the crystal structures of PKA and the Chk1-compound **2** complex unambiguously reveals steric clashes between some PKA side chains and this compound (Figure 5). These clashes would also be present with the other compounds in Table 1 and therefore explain the selectivity between Chk1 and PKA.

A more functionally relevant test regarding selectivity is the comparison of Chk1 inhibition with that of human CDK1. CDK1 activity is needed for cells to go through the G2/M checkpoint and is therefore essential for the therapeutic strategy presented in the Introduction. It follows that ideal Chk1 inhibitors should not target CDK1. The data presented in Table 1 show that compounds in the pyrrolopyrimidine series are as potent against CDK1 as Chk1; however several furanopyrimidine compounds showed a promising degree of selectivity in the desired direction. This suggests that differential selectivity between Chk1 and CDK1 is achievable and could probably be improved with further medicinal chemistry efforts.

Conclusions

We reported here the discovery, synthesis, and crystallographic binding mode of novel furanopyrimidine and pyrrolopyrimidine inhibitors of the Chk1 kinase, which is a target of great therapeutic interest for oncology. In contrast with some other Chk1 inhibitors,

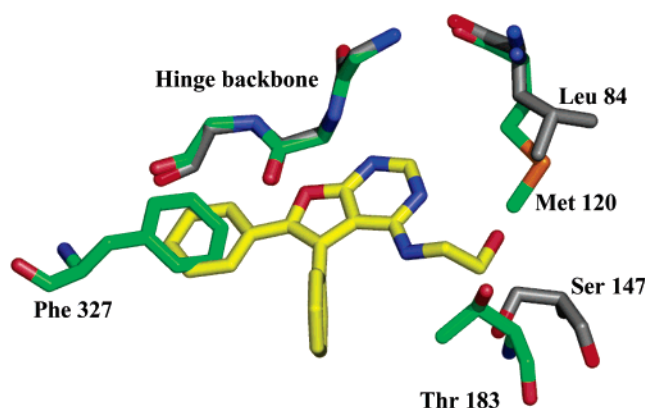


Figure 5. Superposition of the crystal structure of PKA (green carbon atoms, PDB entry 1APM) with Chk1 (gray carbon atoms) in complex with compound **2**. The conserved hinge backbones of both proteins are very closely aligned. The PKA side chains (Met120, Thr183, and Phe327) which would sterically clash with compound **2** are shown and labeled, as well as their counterpart in Chk1. The phenyl ring of Phe327 overlaps with a phenyl ring of compound **2**. The hydroxyl oxygens of Thr183 and of the compound side chain are only 1.9 Å apart. The carbon at the tip of the Met120 side chain (C_{ϵ}) is 1.7 Å from the compound side chain oxygen.

these novel ligands have the advantage of being "drug-like" and can be synthesized without the supply of a natural product.

A chronological account of this work has the merit to illustrate how structural information about the target allowed the formulation and testing of well-defined hypotheses to guide medicinal chemistry. In particular, a few lessons may be gleaned from an objective comparison of the earlier molecular modeling suggestions and the subsequent results from crystallography. Two reasonable model docking modes could be generated quickly at the outset of the project for the newly discovered furanopyrimidine inhibitor. These models helped to prioritize medicinal chemistry efforts, for instance in identifying parts of the ligand which consistently appeared to point toward the solvent. A simple count of presumably favorable polar interactions with the kinase backbone led to the selection of one of these docking modes as the initial preferred working hypothesis. This hypothesis was very convincing in view of a conventional analysis of the ligand–protein interactions and most elements of the SAR available at this stage. Despite these arguments, it was deemed necessary to specifically test this structural model (compound **3**). This test proved crucial in determining that the initial structural model was incorrect. This illustrates the importance of using molecular modeling as part of an iterative cycle of hypothesis generation and rigorous testing. This approach was vindicated when it became apparent that the second docking mode was close to the experimental binding mode determined by crystallography. This experience is of interest for ligand design against kinases in general, given that the possibilities of alternative binding modes are particularly pertinent with these proteins, because of the symmetry of their conserved hinge backbone in the ATP-binding site.⁸³

The crystal structures of the novel furanopyrimidine inhibitors bound to Chk1 provided a firm basis for further elaboration of these compounds. These structures not only explained most of the previously gathered

SAR but led to preparation of the more potent pyrrolopyrimidine analogues. Changing the ligand furan moiety to a pyrrole leads to the formation of one additional regular hydrogen bond between the ligand and the kinase backbone, which translates into a 10-fold increase in affinity. A detailed qualitative analysis of the factors involved, however, indicates that this additional hydrogen bond is expected to contribute only a fraction of the gain in affinity. Such observation may be of general interest, given the ongoing debate about the energetic role of hydrogen bonding in molecular recognition^{74–76} and the rarity of structurally characterized pairs of ligand–protein complexes differing by only one hydrogen bond. This adds credence to the view that the burial of hydrophobic surface area is the main drive for protein–ligand complex formation.

The crystal structures of the present ligand–Chk1 complexes suggest that burying added apolar groups in a nearby pocket could be a strategy to improve the affinity of these compounds for Chk1. This requires derivatization of the hydroxy-ethyl side chain of these compounds from the carbon linked to the hydroxyl group. Indeed, preliminary results showed that the derivatization from this position can be achieved without disruption of the binding mode or degradation of the binding affinities. We suggest that longer substituents specifically designed to reach into this nearby pocket should lead to significant improvements in affinity and presumably selectivity.

Experimental Section

Purchased Compounds. Every purchased compound was subjected to an NMR and liquid chromatography–mass spectrometry analysis to check that they were consistent with the structures shown in Table 2.

2-[5,6-Bis-(4-methoxy-phenyl)-furo[2,3-d]pyrimidin-4-ylamino]-ethanol (1) was purchased from ChemDiv.

5,6-Diphenyl-furo[2,3-d]pyrimidin-4-ylamine (8) was purchased from Chembridge.

3-(5,6-Diphenyl-furo[2,3-d]pyrimidin-4-ylamino)-propan-1-ol (9) was purchased from Chem Div.

Benzyl-(5,6-diphenyl-furo[2,3-d]pyrimidin-4-yl)-amine (10) was purchased from IBS labs.

N-(5,6-Diphenyl-furo[2,3-d]pyrimidin-4-yl)-benzamide (11) was purchased from IBS labs

Synthesis of Furanopyrimidines. This was carried out according to Scheme 1. Compounds **16–19** were prepared according to procedures found in ref 47.

N-(3-Cyano-4,5-diphenyl-furan-2-yl)-formamide (17). Acetic formic anhydride was prepared by heating anhydrous formic acid (60 mL) and acetic anhydride (60 mL) 60 °C for 2 h. The cyanofuran (13.00 g, 50 mmol) was then added to the mixture and heated at 85 °C for 6 h. The reaction mixture was evaporated to about half the original volume and neutralized to pH 6 at 0 °C with 2 M NaOH solution. The precipitate produced was filtered off and dried. This gave the crude product as a white solid (11 g, 72%) that was used without further purification: ¹NMR (CDCl₃) δ 7.27–7.59 (10, m); 8.19 (1H, s); 12.67 (1H, s).

5,6 Diphenyl-3H-furo[2,3-d]pyrimidin-4-one (18). The formamide **17** (3.00 g, 98 mmol) was stirred for 10 min at 220 °C under nitrogen. After the crude material was cooled, it was crystallized from methanol, giving the pure product (2.50 g, 88%) as a white solid: mp >240 °C; MS EI *m/e* 289 (M⁺ + H); ¹NMR (DMSO-*d*₆) δ 7.27–7.59 (10H, m); 8.19 (1H, s); 12.67 (1H, s).

4-Chloro-5,6-diphenyl-furo[2,3-d]pyrimidine (19). The pyrimidone **18** (2.50 g, 8.7 mmol) and phosphorus oxychloride (25 mL) were stirred at 55 °C for 2 h. After this time, the

reaction mixture was poured onto crushed ice (100 g) and neutralized with sodium carbonate solution. The product was then extracted with chloroform and dried over magnesium sulfate. The residue was purified by passing through a silica gel column using chloroform–petroleum ether as the eluent, to afford the product (2.00 g, 75%) as a white solid: mp 121–122 °C; MS EI *m/e* 307 (M⁺ + H); ¹NMR (DMSO-*d*₆) δ 7.25–7.70 (10H, m) 8.86 (1H, s).

Method A: 2-(5,6-Diphenyl-furo[2,3-d]pyrimidin-4-ylamino)-ethanol (2). The chloropyrimidine **19** (0.27 g, 0.88 mmol) and ethanolamine (0.12 g, 1.9 mmol) were refluxed in ethanol with for 8 h. After this time, the reaction was concentrated, and the crude material was purified by passing through a silica gel column using chloroform–petroleum ether as the eluent to afford the product (0.25 g, 86%) as a white solid: mp 163–165 °C; MS EI *m/e* 332 (M⁺ + H); ¹NMR (CDCl₃) δ 3.54–3.64 (2H, m); 3.68–3.78 (2H, m); 3.97–4.75 (1H, m); 5.19 (1H, m); 7.21–7.64 (10H, m); 8.40 (1H, s). Anal. (C₂₀H₁₇N₃O₂) C, H, N.

2-[(5,6-Diphenyl-furo[2,3-d]pyrimidin-4-yl)-methylamino]-ethanol (3). This was prepared according to method A using N-methyl ethanolamine, affording the product as an off-white solid: mp 79–81 °C; MS EI *m/e* 346 (M⁺ + H); ¹NMR (DMSO-*d*₆) δ 2.58 (3H, s); 3.17–3.50 (4H, m); 4.31–4.80 (1H, br. s); 7.25–7.62 (10H, m); 8.32 (1H, s). Anal. (C₂₁H₁₉N₃O₂) H, N, C: calcd, 71.73; found, 73.03.

(5,6-Diphenyl-furo[2,3-d]pyrimidin-4-ylamino)-acetic Acid (4). This was prepared according to method A using glycine, affording the product as an off-white solid: mp >240 °C; MS EI *m/e* 346 (M⁺ + H); ¹NMR (DMSO-*d*₆) δ 2.60 (1H, br); 4.20 (2H, d, *J* = 6 Hz); 5.60 (1H, br); 7.20–7.65 (10H, m); 8.40 (1H, s). Anal. (C₂₁H₁₉N₃O₂) C, H, N.

2-(5,6-Diphenyl-furo[2,3-d]pyrimidin-4-ylamino)-2-phenyl-ethanol (12). This was prepared according to method A using 2-phenyl ethanol, affording the product as an off-white solid: mp 71–73 °C; MS EI *m/e* 408 (M⁺ + H); ¹NMR (CDCl₃) δ 3.66–3.91 (2H, m); 3.76–3.84 (1H, m); 4.24–4.71 (1H, m); 5.19–5.71 (2H, m); 6.90–7.64 (15H, m); 8.39 (1H, s).

N-(5,6-Diphenyl-furo[2,3-d]pyrimidin-4-yl)-ethane-1,2-diamine-trifluoroacetate Salt (13). This was prepared according to method A using (2-amino-ethyl)-carbamic acid *tert*-butyl ester followed by treatment with trifluoroacetic acid. Recrystallization of the product afforded the trifluoroacetate salt as a white solid: mp 196–198 °C (dec); MS EI *m/e* 331 (M⁺ + H); ¹NMR (CDCl₃) δ 3.09–3.25 (2H, br. s); 3.52–3.68 (2H, br.s); 5.09 (1H, m); 7.17–7.64 (11H, m); 8.36 (1H, s); 8.69–9.15 (2H, br. s).

(5,6-Diphenyl-furo[2,3-d]pyrimidin-4-yl)-(2-methoxy-ethyl)-amine (14). This was prepared according to method A using *O*-methylethanolamine affording the product as a white solid: mp 115–117 °C; MS EI *m/e* 346 (M⁺ + H); ¹NMR (DMSO-*d*₆) δ 3.12 (3H, s); 3.24–3.41 (2H, m); 3.44–3.58 (2H, m); 4.31–5.19 (1H, m); 7.28–7.71 (10H, m); 8.35 (1H, s).

Synthesis of Pyrrolopyrimidines. This was carried out according to Scheme 2. **4-Chloro-5,6-diphenyl-7H-pyrrolo[2,3-d]pyrimidine (22).** The commercially available 7-Benzyl-4-chloro-5,6-diphenyl-7H-pyrrolo[2,3-d]pyrimidine (**21**, from Bionet Research) (1.00 g, 2.50 mmol) was suspended in toluene (20 mL). To this was added aluminum trichloride (2.40 g, 18.00 mmol) and the reaction mixture heated to 100 °C overnight. The reaction mixture was cooled and partitioned between water and dichloromethane. The organic layer was then dried and evaporated. The residue was purified by passing through a silica gel column using ethyl acetate–hexane as the eluent to afford the product (0.25 g, 54% based on recovered starting material) as an off-white solid: MS EI *m/e* 345 (M⁺ + H); ¹NMR (DMSO-*d*₆) 7.376–7.5 (10H, m); 9.70 (1H, s).

Method B: 2-(5,6-Diphenyl-7H-pyrrolo[2,3-d]pyrimidin-4-ylamino)-ethanol (5). The chloropyrrolopyrimidine **22** (0.02 g, 0.08 mmol) and ethanolamine (14 μL, 0.24 mmol) were heated to 150 °C under microwave conditions for 60 min. After this time, the solvents were evaporated and the residue was purified by passing through a silica gel column using ethyl acetate as the eluent to afford the product (0.05 g, 20%) as a

solid: mp 245–249 °C; MS EI *m/e* 331 ($M^+ + H$); ^1NMR (CDCl_3) δ 3.50–3.60 (2H, q, $J = 5$ Hz); 3.70–3.75 (2H, m); 5.25–5.30 (1H, m); 7.21–7.45 (10H, m); 8.20 (1H, m); 12.74 (1H, br. s). Anal. ($\text{C}_{20}\text{H}_{18}\text{N}_4\text{O}$) H, N, C: calcd, 72.09; found, 72.71.

1-(5,6-Diphenyl-7H-pyrrolo[2,3-d]pyrimidin-4-ylamino)-propan-2-ol (6). This was prepared according to method B using 1-amino-propan-2-ol, affording the product as solid: mp 257–262 °C; MS EI *m/e* 345 ($M^+ + H$); ^1NMR (CDCl_3) δ 1.20 (3H, d, $J = 6.3$ Hz); 3.30–3.40 (1H, ddd, $J = 14.3, 7.0, 5.5$ Hz); 3.50–3.60 (1H, ddd, $J = 14.0, 6.2, 2.4$ Hz); 3.85–3.95 (1H, m); 5.20–5.25 (1H, m); 7.20–7.50 (10H, m); 8.20 (1H, s); 12.95 (1H, br. s). Anal. ($\text{C}_{21}\text{H}_{20}\text{N}_4\text{O}$) H, N, C: calcd, 72.55; found, 73.23.

3-(5,6-Diphenyl-7H-pyrrolo[2,3-d]pyrimidin-4-ylamino)-propane-1,2-diol (7). This was prepared according to method B using 3-amino-propane-1,2-diol, affording the product as a solid: 228–234 °C; MS EI *m/e* 361 ($M^+ + H$); ^1NMR (CDCl_3) δ 3.48–3.62 (2H, m); 3.68–3.76 (1H, m); 5.15–5.20 (1H, m); 7.20–7.50 (10H, m); 8.20 (1H, s); 12.95 (1H, br. s). Anal. ($\text{C}_{21}\text{H}_{20}\text{N}_4\text{O}_2$) H, N, C: calcd, 67.94; found, 69.98. N: calcd, 15.10; found, 15.54.

Molecular Modeling. Docking was performed with the program rDock which is an extension of the program RiboDock⁸⁴ using an empirical scoring function calibrated based on protein–ligand complexes.^{85,86} The Monte Carlo/simulated annealing protocol initially used in RiboDock was replaced by a steady-state Genetic Algorithm (GA) to improve the efficiency of the docking search. Ligand docking poses were represented using a conventional chromosome representation of translation, rotation, and rotatable bond dihedral angles. A single GA population was used, of size proportional to the number of ligand rotatable bonds, with a mutation/crossover ratio of 3:2. The overall orientation and internal conformation of the compounds were searched with the GA, while the receptor site was kept fixed.

Docking used the ATP-binding site in the crystal structure of apo human Chk1 (protein data bank (PDB)⁸⁷ entry 1IA8). Water molecules were removed from the coordinates, and polar hydrogens were added to the protein using the CHARMM force field.⁸⁸ To specify the docking volume, the ATP-bound crystal structure of PKA (PDB entry 1ATP) was superimposed onto that of Chk1. There was unambiguous superimposition of the ATP-binding sites, and the docking volume in Chk1 was defined as the space within 8 Å of the ATP molecule. Before docking, the three-dimensional (3D) structure of the compounds was built with the software MOE⁸⁹ and energy minimized with the Merck molecular force field.⁹⁰ Each compound was subjected to 200 docking runs, and the output docking modes were analyzed by visual inspection in conjunction with the docking scores.

The MM/PBSA calculations were performed using the program CHARMM,^{91,92} with the protein X-ray structures indicated in Table 4 and Table 5. The partial atomic charges for the compounds were derived by fitting to the molecular electrostatic potential and the dipole moment⁹³ calculated quantum mechanically at the restricted Hartree-Fock/6-31G* level with the program GAMESS.⁹⁴ The CHARMM force field for small organic molecules⁹⁵ was applied to the compounds in combination with the CHARMM all-atom protein force field.⁸⁸ Prior to MM/PBSA calculations, the compounds were energy minimized while keeping the protein nonhydrogen atoms fixed at their X-ray coordinates. The electrostatic contribution ΔG_{elec} to the total free energy of binding $\Delta G_{\text{binding}}$ was obtained with the PBEQ module of CHARMM,⁹⁶ using the Born radii specially derived for this type of calculations.⁹⁷ The aqueous solvent was assigned a dielectric constant of 80.0. Two values of the solute dielectric constant (2 or 4) were used, to test the effect of this parameter on the results. The ionic strength was set to 145 mM and the temperature to 298 K. The electrostatic potentials were calculated using the grid focusing technique, using two successive grids with spacings of 1.0 and 0.3 Å. The first and second grids, extended by at least 20 and 5 Å, respectively, around the complex. The interior

of the solutes was defined as the volume inaccessible to a solvent probe sphere of radius 1.4 Å.⁹⁸ The nonpolar contribution ΔG_{np} of the free energy was calculated as in previously described protocols,^{60,61} which assume that it is proportional ($\gamma = 0.025$ kcal/mol Å²) to the decrease in solvent accessible surface area (SASA) upon complexation

$$\Delta G_{\text{np}} = \gamma(\text{SASA}^{\text{complex}} - (\text{SASA}^{\text{protein alone}} + \text{SASA}^{\text{ligand alone}})) \quad (\text{c})$$

The van der Waals interaction energy between ligand and protein (ΔG_{vdw}) and the ligand relative internal conformational energy ($\Delta G_{\text{internal_rel}}$) also need to be added to the final relative free energy of binding $\Delta G_{\text{binding}}$ when comparing binding modes of a same ligand (Eqn a). $\Delta G_{\text{internal_rel}}$ is the internal energy of the bound ligand relative to that of the free ligand. The thermodynamic cycle used assumes that the conformations of the free and bound ligands are identical. Therefore, the bound conformation of lowest internal energy was taken to represent the reference internal energy of the free ligand, and the $\Delta G_{\text{internal_rel}}$ components were offset relative to this reference.

$\Delta G_{\text{binding}}$ neglects translational, rotational, and vibrational entropy changes upon complexation; however, it is expected that these contributions would be very similar for different binding modes of the same ligand and would cancel out when comparing $\Delta G_{\text{binding}}$ for these binding modes.

Pictures of 3D molecular structures were prepared with PyMOL.⁹⁹

Expression Vector Construction. Amino acids 1–289 of Chk1 were amplified from IMAGE clone 5181427 with primers MoloRT473 (TAC CGG GGA TCC ACC ATG GCA GTG CCC TTT GTG GAA GAC T) and MoloRT474 (GTG TTC CTC GAG TCA TTA GTG GTG GTG ATG GTG ATG GTG GTG TCC ACT GGG AGA CTC TGA CAC ACC) by the polymerase chain reaction (PCR) and subcloned into pCR2.1 using the TopoTA cloning system (Invitrogen) to create the plasmid pCR2.1 Chk1 1–289 C8H. The insert was sequenced to verify that no errors were introduced during the PCR reaction. A 900 bp EcoRI–XhoI fragment from pCR2.1 Chk1 1–289 C8H was subcloned into pFastBac1 to create the plasmid pFastBac1/Chk1 1–289 C8H. Recombinant bacmids were prepared using the Bac-to-Bac system according to the manufacturer's instructions (Invitrogen). Bacmids were confirmed by PCR analysis (data not shown). This bacmid encodes amino acids 1–289 of Chk1 encompassing the kinase domain with a C-terminal 8-His tag.

Chk1 Baculoviral Protein Expression and Purification. Bacmids were transfected in Sf9 cells and used to generate high titer stocks. Expression of Chk1 1–289 C8H was achieved in Sf9 cells with a multiplicity of infection (MOI) of 0.5 for 3 days. Cell pellets were lysed using Popculture (Novagen), and Chk1 was purified with the following scheme. The initial step performed was Q-Sepharose, followed by Ni-affinity, hydrophobic interaction chromatography (using Source-Phenol), and finally gel filtration. This provided us with >95% pure protein. However, we routinely obtained low yields with this construct (< 1 mg of purified Chk1/L of Sf9 cells) presumably because of the high endogenous activity of the isolated kinase domain of Chk1.⁴²

Chk1 Kinase Assay. Compounds were titrated in a twofold dilution series in 100% DMSO in a 96-well plate (V-bottom clear plate, VWR 007/008/257) at 50 times the final concentration. Subsequently, 1 μL of this series was added to a separate 96-well plate, to which a mixture of 10 μL of buffer (250 mM HEPES–NaOH, pH 7.5), 0.5 μL of BSA (10 mg/mL), 2 μL of Chktide (1 mg/mL), 0.5 μL of full-length Chk1 enzyme (10 mM), and 26 μL of double-distilled water was added per well. To start the assay, a second mixture of 0.75 μL of 1M magnesium acetate, 0.05 μL of ATP (100mM), 0.05 μL of ^{33}P γ -ATP (assuming specific activity of 10 mCi/mL), and 9.15 μL of double-distilled water was added per well. The control wells contained 1 μL of 100% DMSO or 1 μL of 50 μM Staurosporine (Calbiochem #569397) to give a final concentration of 1 μM . The assay was incubated for 30 °C for 40 min. The reaction was stopped by adding 50 μL of 50 mM phosphoric acid, and

90 μ L of the stopped assay plate was transferred to a pre-wet phospho-cellulose filter plate (Millipore MAPHNOB50). The filter plate was then vacuum filtered, washed three times with phosphoric acid and once with methanol, and dried at 65 °C. Scintillation fluid (50 μ L) (National Diagnostics LS-273) was added per well, and the plate was counted on a Perkin-Elmer Trilux scintillation counter. The limit of detection for this assay is 5 nM and typical Z values are >0.7.

CDK1 and PKA Assays. Assays with human CDK1 and PKA were performed in a manner similar to that of the Chk1 assay. For the CDK1 assay, 8 ng CDK1 enzyme were used with 30 μ M Histone H1 as a substrate with a final ATP concentration of 100 μ M. The CDK1 assay was incubated at 30 °C for 40 min. For the PKA assay, 10 units of PKA enzyme (Upstate) were used with 0.75 μ M Kemptide as a substrate with a final ATP concentration of 100 μ M. The PKA assay was incubated at 30 °C for 30 min.

Crystallization and 3D Structure Determination. Chk1 protein was concentrated to 3 mg/mL using ultrafiltration into a final buffer containing 25 mM Tris pH 7.5, 0.5 M NaCl, and 1 mM DTT. Apo-Chk1 crystals were grown using crystallization conditions containing 10–15% PEG8K, 0.1 M Hepes pH 7.5, and 15% (v/v) 2-propanol. To obtain a crystal of Chk1 in complex with a ligand, this ligand was soaked into an apo crystal. Single crystals were removed from the apo-protein crystallization drops and placed in a solution of 4 μ L of crystallization reservoir plus 0.5 μ L of ligand stock solution. The ligand stock solution was 20 mM in 100% DMSO. The crystals were left to soak at 18 °C for a period of approximately 16 h.

The complex data sets were collected at cryotemperature. The cryoprotectant used was the same as the reservoir solution from which the crystals grew except 20% glycerol was added. Data were collected on beamline 19-ID at the APS (Chicago) or beamline ID29 at the ESRF (Grenoble) and were subsequently processed using DENZO,¹⁰⁰ in $P2_1$ space group with unit-cell dimensions isomorphous to those of the previously solved apo-Chk1 structure.⁴² Hence, the ligand-bound structures were solved by isomorphous replacement using the apo-Chk1 model coordinates and the refinement program REFMAC5.¹⁰¹ Twenty cycles of rigid-body refinement followed by twenty cycles of restrained refinement were carried out. All model building was carried out using the molecular graphics program O,¹⁰² and refinement calculations were performed by REFMAC5. Difference electron density maps were calculated for the initial model and inspected following the structure solution. Crystallographic water molecules were added by cycling REFMAC5 with ARP/wARP.¹⁰³ After each round of refinement, the models were adjusted and further solvent molecules were gradually added. The progress of the refinement was assessed using R_{free} and the conventional R factor. Once refinement of the structure had converged and the R_{free} and R factor could not be lowered further, the structures were validated using PROCHECK¹⁰⁴ and various programs from the CCP4i package.¹⁰⁵ Full data collection and refinement statistics are presented in Table 3.

Acknowledgment. We thank the support staff of beamlines ID29 at the European Synchrotron Radiation Source, Grenoble, France and 19-ID at the Advanced Photon Source, Chicago, IL, USA for help with data collection. We also thank A. Hold for analytical chemistry support, and Pr. R. Hubbard for helpful comments on the manuscript.

Supporting Information Available: Elemental analysis for key target compounds. This material is available free of charge via the Internet at <http://pubs.acs.org>.

References

- Hanahan, D.; Weinberg, R. A. The Hallmarks of Cancer. *Cell* **2000**, *100*, 57–70.
- Nurse, P. Checkpoint Pathways Come of Age. *Cell* **1997**, *91*, 865–867.
- Zhou, B.-B.; Elledge, S. J. The DNA Damage Response: Putting Checkpoints in Perspective. *Nature* **2000**, *408*, 433–439.
- Melo, J.; Toczyski, D. A unified view of the DNA-damage checkpoint. *Curr. Opin. Cell Biol.* **2002**, *14*, 237–245.
- Kastan, M. B.; Onyekwere, O.; Sidransky, D.; Vogelstein, B.; Craig, R. W. Participation of p53 protein in the cellular response to DNA damage. *Cancer Res.* **1991**, *51*, 6304–6311.
- Li, Q.; Zhu, G.-D. Targeting Serine/Threonine Protein Kinase B/Akt and Cell-cycle Checkpoint Kinases for Treating Cancer. *Curr. Top. Med. Chem.* **2002**, *2*, 939–971.
- Greenblatt, M. S.; Bennett, W. P.; Hollstein, M.; Harris, C. C. Mutations in the p53 tumor suppressor gene: clues to cancer etiology and molecular pathogenesis. *Cancer Res.* **1994**, *54*, 4855–4878.
- Wang, Q.; Fan, S.; Eastman, A.; Worland, P. J.; Sausville, E. A.; et al. UCN-01: a potent abrogator of G₂ checkpoint function in cancer cells with disrupted p53. *J. Natl. Cancer Inst.* **1996**, *88*, 956–965.
- Bunch, R. T.; Eastman, A. Enhancement of Cisplatin-induced Cytotoxicity by 7-Hydroxystaurosporine (UCN-01), a New G₂–Checkpoint Inhibitor. *Clin. Cancer Res.* **1996**, *2*, 791–797.
- Tenzer, A.; Pruschy, M. Potentiation of DNA-Damage-Induced Cytotoxicity by G₂ Checkpoint Abrogators. *Curr. Med. Chem.* **2003**, *3*, 35–46.
- Shao, R.-G.; Cao, C.-X.; Shimizu, T.; O'Connor, P. M.; Kohn, K. W.; et al. Abrogation of an S–Phase Checkpoint and Potentiation of Camptothecin Cytotoxicity by 7-Hydroxystaurosporine (UCN-01) in Human Cancer Cell Lines, Possibly Influenced by p53 Function. *Cancer Res.* **1997**, *57*, 4029–4035.
- Jin, P.; Gu, Y.; Morgan, D. O. Role of inhibitory CDC2 phosphorylation in radiation-induced G₂ arrest in human cells. *J. Cell Biol.* **1996**, *134*, 963–970.
- Poon, R. Y. C.; Jiang, W.; Toyoshima, H.; Hunter, T. Cyclin-dependent kinases are inactivated by a combination of p21 and Thr-14/Tyr-15 phosphorylation after UV-induced DNA damage. *J. Biol. Chem.* **1996**, *271*, 13283–13291.
- Rhind, N.; Furnari, B.; Russell, P. Cdc2 tyrosine phosphorylation is required for the DNA damage checkpoint in fission yeast. *Genes Dev.* **1997**, *11*, 504–511.
- Millar, J. B. A.; Blevitt, J.; Gerace, L.; Sadhu, K.; Featherstone, C.; et al. p53^{CDC25} is a nuclear protein required for the initiation of mitosis in human cells. *Proc. Natl. Acad. Sci. U.S.A.* **1991**, *88*, 10500–10504.
- Lee, M. S.; Ogg, S.; Xu, M.; Parker, L. L.; Donoghue, D. J.; et al. cdc25+ encodes a protein phosphatase that dephosphorylates p34^{cdc2}. *Mol. Biol. Cell* **1992**, *3*, 73–84.
- Sanchez, Y.; Wong, C.; Thoma, R. S.; Richman, R.; Wu, Z.; et al. Conservation of the Chk1 Checkpoint Pathway in Mammals: Linkage of DNA Damage to Cdk Regulation Through Cdc25. *Science* **1997**, *277*, 1497–1501.
- Peng, C.-Y.; P. R., G.; Thoma, R. S.; Wu, Z.; Shaw, A. S.; et al. Mitotic and G₂ Checkpoint Control: Regulation of 14–3–3 Protein Binding by Phosphorylation of Cdc25C on Serine-216. *Science* **1997**, *5*, 1501–1505.
- Chen, P.; Gatei, M.; O'Connell, M. J.; Khanna, K. K.; Bugg, S. J.; et al. Chk1 complements the G₂/M checkpoint defect and radiosensitivity of ataxia-telangiectasia cells. *Oncogene* **1999**, *18*, 249–256.
- Luo, Y.; Rockow-Magone, S. K.; Kroeger, P. E.; Frost, L.; Chen, Z.; et al. Blocking CHK1 Expression Induces Apoptosis and Abrogates the G₂ Checkpoint Mechanism. *Neoplasia* **2001**, *3*, 411–419.
- Takai, H.; Tominaga, K.; Motoyama, N.; Minamishima, Y. A.; Nagahama, H.; et al. Aberrant cell cycle checkpoint function and early embryonic death in Chk1 $-/-$ mice. *Genes Dev.* **2000**, *14*, 1439–1447.
- Furnari, B.; Rhind, N.; Russell, P. Cdc25 Mitotic Inducer Targeted by Chk1 DNA Damage Checkpoint kinase. *Science* **1997**, *277*, 1495–1497.
- Liu, Q.; Guntuku, S.; Cui, X. S.; Matsuoka, S.; Cortez, D.; et al. Chk1 is an essential kinase that is regulated by Atr and required for the G₂/M DNA damage checkpoint. *Genes Dev.* **2000**, *14*, 2448–2459.
- Zhao, H.; Piwnicka-Worms, H. ATR-mediated checkpoint pathways regulate phosphorylation and activation of human Chk1. *Mol. Biol. Cell* **2001**, *21*, 4129–4139.
- Lopez-Girona, A.; Tanaka, K.; Chen, X.-B.; Baber, B. A.; McGowan, C. H.; et al. Serine-345 is required for Rad3-dependent phosphorylation and function of checkpoint kinase Chk1 in fission yeast. *Proc. Natl. Acad. Sci. U.S.A.* **2001**, *98*, 11289–11294.
- Guo, Z. J.; Kumagai, A.; Wang, S. X.; Dunphy, W. G. Requirement for Atr in phosphorylation of Chk1 and cell cycle regulation in response to DNA replication blocks and UV-damaged DNA in *Xenopus* egg extracts. *Genes Dev.* **2000**, *14*, 2745–2756.
- Capasso, H.; Palermo, C.; Wan, S.; Rao, H.; John, U. P.; et al. Phosphorylation activates Chk1 and is required for Checkpoint-mediated cell cycle arrest. *J. Cell Sci.* **2002**, *115*, 4555–4564.

- (28) Rhind, N.; Russell, P. Chk1 and Cds1: linchpins of the DNA damage and replication checkpoint pathways. *J. Cell Sci.* **2000**, *113*, 3889–3896.
- (29) Chen, Z.; Xiao, Z.; Chen, J.; Ng, S.-C.; Sowin, T.; et al. Human Chk1 Expression Is Dispensable for Somatic Cell Death and Critical for Sustaining G₂ DNA Damage Checkpoint. *Mol. Cancer Ther.* **2003**, *2*, 543–548.
- (30) Zachos, G.; Rainey, M. D.; Gillespie, D. A. F. Chk1-deficient tumour cells are viable but exhibit multiple checkpoint and survival defects. *EMBO J.* **2003**, *22*, 713–723.
- (31) Graves, P. R.; Yu, L.; Schwarz, J. K.; Gales, J.; Sausville, E. A.; et al. The Chk1 Protein Kinase and the Cdc25C Regulatory Pathways are Targets of the Anticancer Agent UCN-01. *J. Biol. Chem.* **2000**, *275*, 5600–5605.
- (32) Busby, E. C.; Leistriz, D. F.; Abraham, R. T.; Karnitz, L. M.; Sarkaria, J. N. The Radiosensitizing Agent 7-Hydroxystaurosporine (UCN-01) Inhibits the DNA Damage Checkpoint Kinase hChk1. *Cancer Res.* **2000**, *2000*, 2108–2112.
- (33) Jackson, J. R.; Gilmartin, A.; Imburgia, C.; Winkler, J. D.; Marshall, L. A.; et al. An Indolocarbazole Inhibitor of Human Checkpoint Kinase (Chk1) Abrogates Cell Cycle Arrest Caused by DNA Damage. *Cancer Res.* **2000**, *60*, 566–572.
- (34) Eastman, A.; Kohn, E. A.; Brown, M. K.; Rathman, J.; Livingstone, M.; et al. A Novel Indolocarbazole, ICP-1, Abrogates DNA Damage-induced Cell Cycle Arrest and Enhances Cytotoxicity: Similarities and Differences to the Cell Cycle Checkpoint Abrogator UCN-01. *Mol. Cancer Ther.* **2002**, *1*, 1067–1078.
- (35) Roberge, M.; Berlinck, R. G. S.; Xu, L.; Anderson, H. J.; Lim, L. Y.; et al. High-throughput assay for G₂ checkpoint inhibitors and identification of the structurally novel compound isogranulatimide. *Cancer Res.* **1998**, *58*, 5701–5706.
- (36) Kohn, E. A.; Yoo, C. J.; Eastman, A. The Protein Kinase C Inhibitor Gö6976 Is a Potent Inhibitor of DNA Damage-induced S and G₂ Cell Cycle Checkpoints. *Cancer Res.* **2003**, *63*, 31–35.
- (37) Curman, D.; Cinel, B.; Williams, D. E.; Rundle, N.; Block, W. D.; et al. Inhibition of the G₂ DNA Damage Checkpoint and of Protein Kinases Chk1 and Chk2 by the Marine Sponge Alkaloid Debromohymenialdisine. *J. Biol. Chem.* **2001**, *276*, 17914–17919.
- (38) Sausville, E. A.; Arbuck, S. G.; Messmann, R.; Headlee, D.; Lush, R. D.; et al. Phase I Trial of 72-Hour Continuous Infusion UCN-01 in Patients with Refractory Neoplasms. *J. Clin. Oncol.* **2001**, *19*, 2319–2333.
- (39) Senderowicz, A. M. The Cell Cycle as a Target for Cancer Therapy: Basic and Clinical Findings with the Small Molecule Inhibitors Flavopiridol and UCN-01. *Oncologist* **2002**, *7*, 12–19.
- (40) Lyne, P. D.; Kenny, P. W.; Cosgrove, D. A.; Deng, C.; Zabudoff, S.; et al. Identification of Compounds with Nanomolar Binding Affinity for Checkpoint Kinase-1 Using Knowledge-Based Virtual Screening. *J. Med. Chem.* **2004**, *47*, 1962–1968.
- (41) Kania, R. S.; Bender, S. L.; Borchardt, A.; Braganza, J. F.; Cripps, S. J.; et al. Indazole compounds and pharmaceutical compositions for inhibiting protein kinases and methods for their use. Patent WO 0102369, 2001.
- (42) Chen, P.; Luo, C.; Deng, Y.; Ryan, K.; Register, J.; et al. The 1.7 Å Crystal Structure of Human Cell Cycle Checkpoint Kinase Chk1: Implications for Chk1 Regulation. *Cell* **2000**, *100*, 681–692.
- (43) Zhao, B.; Bower, M. J.; McDevitt, P. J.; Zhao, H.; Davis, S. T.; et al. Structural Basis for Chk1 Inhibition by UCN-01. *J. Biol. Chem.* **2002**, *277*, 46609–46615.
- (44) <http://www.chemdiv.com>.
- (45) Baurin, N.; Baker, R.; Richardson, C.; Chen, I.; Foloppe, N.; et al. Drug-like annotation and duplicate analysis of a 23-supplier chemical database totalling 2.7M compounds. *J. Chem. Inf. Comput. Sci.* **2004**, *44*, 643–651.
- (46) <http://mdli.com>.
- (47) Johannsen, F.; Jorgensen, A.; Pedersen, E. B. Reactions of Heterocyclic α -Aminonitriles with Acetic Formic Anhydride. *Chim. Scripta* **1986**, *26*, 347–351.
- (48) Toledo, L. M.; Lydon, N. B.; Elbaum, D. The Structure-Based Design of ATP-Site Directed Protein Kinase Inhibitors. *Curr. Med. Chem.* **1999**, *6*, 775–805.
- (49) Noble, M. E.; Endicott, J. A.; Johnson, L. N. Protein Kinase Inhibitors: Insights into Drug Design from Structure. *Science* **2004**, *303*, 1800–1805.
- (50) Williams, D. H.; Mitchell, T. Latest developments in crystallography and structure-based design of protein kinase inhibitors as drug candidates. *Curr. Opin. Pharmacol.* **2002**, *2*, 567–573.
- (51) Steiner, T. Donor and acceptor strengths in C–H...O hydrogen bonds quantified from crystallographic data of small solvent molecules. *New J. Chem.* **1998**, 1099–1103.
- (52) Pierce, A. C.; Sandretto, K. L.; Bemis, G. W. Kinase Inhibitors and the Case for CH...O Hydrogen Bonds in Protein–Ligand Binding. *Proteins* **2002**, *49*, 567–576.
- (53) Desiraju, G. R.; T., S. *The Weak Hydrogen Bond In Structural Chemistry and Biology*; Oxford Science Publications: New York, 1999.
- (54) Levitt, M.; Perutz, M. F. Aromatic Rings Act as Hydrogen Bond Acceptors. *J. Mol. Biol.* **1988**, *201*, 751–754.
- (55) Meyer, E. A.; Castellano, R. K.; Diederich, F. Interactions with Aromatic Rings in Chemical and Biological Recognition. *Angew. Chem.* **2003**, *42*, 1210–1250.
- (56) Steiner, T.; Koellner, G. Hydrogen Bonds with pi-Acceptors in Proteins: Frequencies and Role in Stabilizing Local 3D Structure. *J. Mol. Biol.* **2001**, *305*, 535–557.
- (57) Böhm, H. J.; Stahl, M. The use of Scoring Functions in Drug Discovery Applications. *Reviews in Computational Chemistry*; Wiley-VCH: New York, 2002; pp 41–87.
- (58) Thomas, K. A.; Smith, G. M.; Thomas, T. B.; Feldmann, R. J. Electronic distributions within protein phenylalanine aromatic rings are reflected by the three-dimensional oxygen atom environments. *Proc. Natl. Acad. Sci. U.S.A.* **1982**, *79*, 4843–4847.
- (59) Kollman, P. A.; Massova, I.; Reyes, C.; Kuhn, B.; Huo, S.; et al. Calculating Structures and Free Energies of Complex Molecules: Combining Molecular Mechanics and Continuum Models. *Acc. Chem. Res.* **2000**, *33*, 889–897.
- (60) Hünenberger, P. H.; Helms, V.; Narayana, N.; Taylor, S. S.; McCammon, J. A. Determinants of Ligand Binding to cAMP-Dependent Protein Kinase. *Biochemistry* **1999**, *38*, 2358–2366.
- (61) Sirockin, F.; Sich, C.; Improta, S.; Schaefer, M.; Saudek, V.; et al. Structure Activity Relationship by NMR and by Computer: A Comparative Study. *J. Am. Chem. Soc.* **2002**, *124*, 11073–11084.
- (62) Halgren, T. Merck Molecular Force Field. I. Basis, Form, Scope, Parametrization, and Performance of MMFF94. *J. Comput. Chem.* **1996**, *17*, 490–519.
- (63) Perola, E.; Charifson, P. S. Conformational Analysis of Drug-Like Molecules Bound to Proteins: An Extensive Study of Ligand Reorganization upon Binding. *J. Med. Chem.* **2004**, *47*, 2499–2510.
- (64) Dunitz, J. D. The Entropic Cost of Bound Water in Crystals and Biomolecules. *Science* **1994**, *264*, 670–670.
- (65) Dill, K. A. Dominant forces in protein folding. *Biochemistry* **1990**, *29*, 7133–7155.
- (66) Fersht, A.; Shi, J. P.; Knill-Jones, J. W.; Lowe, D. M.; Wilkinson, A. J.; et al. Hydrogen bonding and biological specificity analysed by protein engineering. *Nature* **1985**, *314*, 235–238.
- (67) Bartlett, P. A.; Marlowe, C. K. Evaluation of Intrinsic Binding Energy from a Hydrogen Bonding Group in an Enzyme Inhibitor. *Science* **1987**, *235*, 569–571.
- (68) Tronrud, D. E.; Holden, H. M.; Matthews, B. W. Structure of Two Thermolysin-Inhibitor Complexes That differ by a Single Hydrogen Bond. *Science* **1987**, *235*, 571–574.
- (69) Fersht, A. The hydrogen bond in molecular recognition. *Trends Biochem. Sci.* **1987**, *12*, 301–304.
- (70) Fersht, A. Relationships between Apparent Binding Energies Measured in Site-Directed Mutagenesis Experiments and Energetics of Binding and Catalysis. *Biochemistry* **1988**, *27*, 1577–1580.
- (71) Williams, D. H.; Searle, M. S.; Mackay, J. P.; Gerhard, U.; Maplestone, R. A. Toward an estimation of binding constants in aqueous solution: Studies of associations of vancomycin group antibiotics. *Proc. Natl. Acad. Sci. U.S.A.* **1993**, *90*, 1172–1178.
- (72) Connelly, P. R.; Aldape, R. A.; Bruzzese, F. J.; Chambers, S. P.; Fitzgibbon, M. J.; et al. Enthalpy of hydrogen bond formation in a protein–ligand binding reaction. *Proc. Natl. Acad. Sci. U.S.A.* **1994**, *91*, 1964–1968.
- (73) Abraham, M. H.; Duce, P. P.; Prior, D. V.; Barrat, D. G.; Morris, J. J.; et al. Hydrogen Bonding. Part 9. Solute Proton Donor and Proton Acceptor Scales for Use in Drug Design. *J. Chem. Soc., Perkin Trans. 2* **1989**, 1355–1375.
- (74) Tame, J. R. H. Scoring functions: A view from the bench. *J. Comput.-Aided Mol. Des.* **1999**, *13*, 99–108.
- (75) Davis, A. M.; Teague, S. J. Hydrogen Bonding, Hydrophobic Interactions, and Failure of the Rigid Receptor Hypothesis. *Angew. Chem., Int. Ed.* **1999**, *38*, 736–749.
- (76) Kubinyi. Hydrogen Bonding, the Last Mystery in Drug Design? *Pharmacokinetic Optimization in Drug Research. Biological, Physicochemical, and Computational Strategies*; Helvetica Chimica Acta and Wiley-VCH: Zürich, Switzerland, 2001; pp 513–524.
- (77) Williams, D. H.; Westwell, M. S. Aspects of weak interactions. *Chem. Soc. Rev.* **1998**, *27*, 57–63.
- (78) Sippl, M. J. Helmholtz Free Energy of Peptide Hydrogen Bonds in Proteins. *J. Mol. Biol.* **1996**, *260*, 644–648.
- (79) Gidofalvi, G.; Wong, C. F.; McCammon, J. A. Entropy Loss of Hydroxyl Groups of Balanol upon Binding to Protein Kinase A. *J. Chem. Educ.* **2002**, *79*, 1122–1126.
- (80) Böhm, H. J.; Brode, S.; Hesse, U.; Klebe, G. Oxygen and Nitrogen in Competitive Situations: Which Is The Hydrogen-Bond Acceptor? *Chem. –Eur. J.* **1996**, *2*, 1509–1513.
- (81) Honig, B.; Sharp, K.; Yang, A.-S. Macroscopic Models of Aqueous Solutions: Biological and Chemical Applications. *J. Phys. Chem.* **1993**, *97*, 1101–1109.

- (82) Manning, G.; Whyte, D. B.; Martinez, R.; Hunter, T.; Sudarsanam, S. The Protein Kinase Complement of the Human Genome. *Science* **2002**, *298*, 1912–1934.
- (83) Furet, P.; Meyer, T.; Strauss, A.; Raccuglia, S.; Rondeau, J.-M. Structure-Based Design and Protein X-ray Analysis of a Protein Kinase Inhibitor. *Bioorg. Med. Chem. Lett.* **2002**, *12*, 221–224.
- (84) Morley, S. D.; Afshar, M. Validation of an empirical RNA-ligand scoring function for fast flexible docking using RiboDock. *J. Comput.-Aided Mol. Des.* **2004**, *18*, 189–208.
- (85) Barril, X.; Hubbard, R. E.; Morley, D. Virtual Screening in Structure-Based Drug Discovery. *Mini-Rev. Med. Chem.* **2004**, *4*, 779–791.
- (86) Morley, D. Unpublished work.
- (87) Berman, H. M.; Westbrook, J.; Feng, Z.; Gilliland, G.; Bhat, T. N.; et al. The Protein Data Bank. *Nucleic Acids Res* **2000**, *28*, 235–242.
- (88) MacKerell, A. D., Jr.; Bashford, D.; Bellott, M.; Dunbrack, R. L., Jr.; Evanseck, J. D.; et al. All-Atom Empirical Potential for Molecular Modeling and Dynamics Studies of Proteins. *J. Phys. Chem. B* **1998**, *102*, 3586–3616.
- (89) <http://www.chemcomp.com>.
- (90) Halgren, T. MMFF VI. MMFF94s Option for Energy Minimization Studies. *J. Comput. Chem.* **1999**, *20*, 720–729.
- (91) Brooks, B. R.; Brucoleri, R. E.; Olafson, B. D.; States, D. J.; Swaminathan, S.; et al. CHARMM: A Program for Macromolecular Energy, Minimization and Dynamics calculations. *J. Comput. Chem.* **1983**, *4*, 187–217.
- (92) <http://www.accelrys.com>.
- (93) Spackman, M. A. Potential Derived Charges Using a Geodesic Point Selection Scheme. *J. Comput. Chem.* **1996**, *17*, 1–18.
- (94) Schmidt, M. W.; Baldrige, K. K.; Boatz, J. A.; Elbert, S. T.; Gordon, M. S.; et al. General Atomic and Molecular Electronic Structure System. *J. Comput. Chem.* **1992**, *13*, 1347–1363.
- (95) Momany, F. A.; Rone, R. Validation of the General Purpose QUANTA 3.2/CHARMM Force Field. *J. Comput. Chem.* **1992**, *13*, 888–900.
- (96) Im, W.; Beglov, D.; Roux, B. Continuum Solvation Model: computation of electrostatic forces from numerical solutions to the Poisson–Boltzmann equation. *Comput. Phys. Commun.* **1998**, *111*, 59–75.
- (97) Nina, M.; Beglov, D.; Roux, B. Atomic radii for continuum electrostatics based on molecular free energy simulations. *J. Phys. Chem. B* **1997**, *101*, 5239–5248.
- (98) Lee, B.; Richards, F. M. The interpretation of protein structures: Estimation of static accessibility. *J. Mol. Biol.* **1971**, *55*, 379–400.
- (99) Delano, W. L. *The PyMOL User's Manual*; DeLano Scientific: San Carlos, CA, 2002.
- (100) Otwinowski, Z.; Minor, W. Processing of X-ray Diffraction Data Collected in Oscillation Mode. *Methods Enzymol.* **1997**, *276*, 307–326.
- (101) Murshudov, G. N.; Vagin, A. A.; Dodson, E. J. Refinement of Macromolecular Structures by the Maximum-Likelihood Method. *Acta Crystallogr.* **1997**, *D53*, 240–255.
- (102) Jones, T. A.; Kjeldgaard, M. O. Version 6.1.2, the manual; Uppsala, Sweden, **1993**.
- (103) Perrakis, A.; Morris, R. J. H.; Lamzin, V. S. Automated protein model building combined with iterative structure refinement. *Nature Struct. Biol.* **1999**, *6*, 458–463.
- (104) Laskowski, R. A.; MacArthur, M. W.; Moss, D. S.; Thornton, J. M. PROCHECK – a program to check the stereochemical quality of protein structures. *J. Appl. Crystallogr.* **1993**, *26*, 283–291.
- (105) Collaborative Computational Project, N. The CCP4 Suite: Programs for Protein Crystallography. *Acta Crystallogr.* **1994**, *D50*, 760–763.

JM049022C